A Journal of the Gesellschaft Deutscher Chemiker

Angewandte International Edition GDCh Chemie

www.angewandte.org

Accepted Article

Title: Cofactor-substrate-based Reporter for Enhancing Signalling Communications towards Hypoxia Enzyme Expression

Authors: Yang Jiao, Lei Zhang, Xu Gao, Wen Si, and Chunying Duan

To be cited as: *Angew. Chem. Int. Ed.* 10.1002/anie.201915040
Angew. Chem. 10.1002/ange.201915040

Link to VoR: http://dx.doi.org/10.1002/anie.201915040
http://dx.doi.org/10.1002/ange.201915040

WILEY-VCH

10.1002/anie.201915040

RESEARCH ARTICLE

WILEY-VCH

Cofactor-substrate-based Reporter for Enhancing Signalling Communications towards Hypoxia Enzyme Expression

Yang Jiao, Lei Zhang, Xu Gao, Wen Si and Chunying Duan*

Abstract: Identifying the location and expression levels of hypoxic enzymes in cancer cells is vital in early-stage cancer diagnosis and efficacy monitoring. By encapsulating a fluorescent substrate, **L-NO$_2$**, within the NADH mimic-containing metal-organic capsule Zn-**MPB**, we developed a new reporter platform named as the cofactor-substrate-based supramolecular luminescent probe for ultrafast detection of hypoxic enzymes in solution *in vitro* and *in vivo*. The host-guest structure directly fuses the coenzyme and substrate into one supramolecular probe to avoid control by NADH, switching the catalytic process of nitroreductase from a complex double-substrate mechanism to a single-substrate one. This probe promotes natural enzyme efficiency by altering the substrate catalytic process and enhances the electron transfer efficiency *via* a promising intra-molecular pathway with increased activity. The enzyme content and fluorescence intensity showed a linear relationship and ultrafast equilibrium was obtained in seconds, showing potential for early tumor diagnosis, biomimetic catalysis, and prodrug activation.

Introduction

Hypoxia, defined as a reduction in the average tissue oxygen tension, is an important indicator of some cancers that disturb the microcirculation[1] and is closely related to various physiological activities of tumors[2,3]. Identifying the location and expression levels of hypoxic enzymes in live cancer cells using molecularly targeted hypoxia-activated methods is essential in early-stage cancer diagnosis and efficacy monitoring[4]. Recent advances in these fields have demonstrated several outstanding substrate-based enzymatic fluorescent probes[5] for detecting and imaging abnormal levels of hypoxic enzymes in solution and live cancer cells through their high sensitivity, non-destructive analysis, and real-time detection abilities[6]. Notably, in early-stage diagnoses of cancers, the concentration and expression levels of the hypoxic enzymes often varied widely in different cells and tumors[7]. Quantitatively detecting and accurately distinguishing the changes in enzyme activity over a wide range between healthy and diseased states remains challenging. Because the different and unknown levels of cofactors and enzymes cause considerable variations in probe emission over time, the fluorescence response rarely shows a distinct and stable linear relationship with the enzyme content.

These cofactor-dependent hypoxia enzymes universally need small-molecule cofactors, redox carriers of biosynthetic reaction[8], to accomplish enzymatic reactions with substrates (or probes)[9], and the cofactor levels have high effect on enzyme kinetics and the detection precision of hypoxia enzyme[10] content. Only if the concentration and diffusion processes of the cofactors were maintained at sufficient level, the enzyme content and the luminescent responses would potentially exhibit a linear relationship. A large excess of cofactor related to the substrate-based probe was always added in the solution to enable the precise and quick detection of enzyme content[11]. However, in different living cells and even in the same cells with different hypoxia conditions, the expression levels of hypoxia enzymes and corresponding cofactors are diverse and indefinite[12], such that the detection of enzyme content in *vivo* was highly dependent on the content of cofactors[13], that is also affected by the hypoxic condition. The combination of substrate-based probe and cofactor into one supramolecular system with clarified stoichiometric ratio between them would render the probe reacting rate almost independent from the cofactor supply, which is beneficial for rapid quantitative detection.

To echo the remarkable properties of enzymes for achieving efficient chemical conversions, chemists have used metal-organic cages with defined hydrophobic cavities as unique hosts to catalyze unique chemical transformations[14,15]. The direct modulation of mimics of cofactors into the backbone of the capsules is postulated to be a promising approach to enforce active sites into close proximity with substrates[16] and promote the electron transfer process between reactants efficiently. The encapsulation of a substrate-based luminescent probe in stoichiometric cofactor-backbone 'molecular containers'[17] would be an important tool for distinguishing and quantitatively detecting different degrees of the enzymatic activity between healthy and diseased states. The new host-guest cofactor-substrate-based supramolecular probe approach enabled the redox reaction of luminescent substrate, cofactor and enzyme to occur efficiently with excellent compatibility between kinetics and reaction intermediates[18].

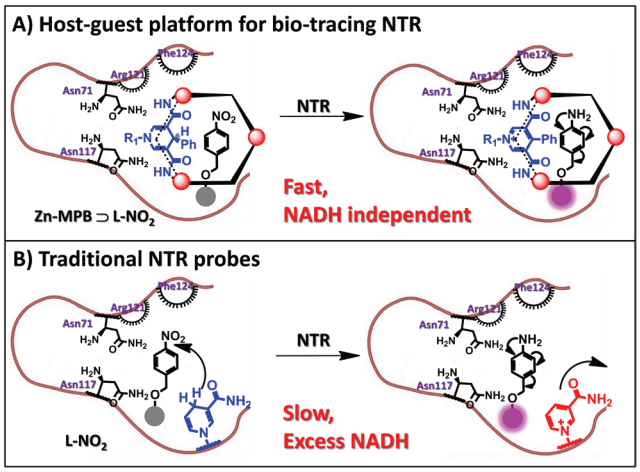

Scheme 1. Schematic of the cofactor-substrate-based supramolecular probe for NTR imaging process.

[*] Dr. Jiao, L. Zhang, X. Gao, W. Si, Prof. C. Duan
State Key Laboratory of Fine Chemicals
Dalian University of Technology,
Dalian City, 116024, China
E-mail: cyduan@dlut.edu.cn

Supporting information and the ORCID identification number(s) for the author(s) of this article can be found under:
https://doi.org/10.1002/anie.201915040

By incorporating the NADH mimics, the most common cofactor[19] in the hypoxic enzymes, into the backbone of a metal-organic capsule Zn-**MPB**, herein we present a cofactor-substrate-based supramolecular probe (Zn-**MPB⊃L-NO$_2$**) for biochemical imaging of hypoxia enzyme nitroreductase (NTR) in aqueous solution and living systems.[20,21] We envisioned that the stoichiometric supply of the cofactor would modify the original multi-substrate enzymatic process of a substrate-based probe into a simpler pseudo-single-substrate kinetic, following the Michaelis–Menten equation. The linear relationship between fluorescence intensity and enzyme content was expected to reach an ultrafast equilibrium in hypoxia enzyme detection with removal of the cofactor content effect (Scheme 1)[13]. In the meantime, the inclusion of the substrate within the NADH–containing host would reduce the transport time of the external NADH and increase the proximity between substrate and the active sites of the cofactor[22], thus enabling the rapidly signalling communication towards hypoxia enzyme expression.

Results and Discussion

The guest molecular probe, **L-NO$_2$**, comprised a nitrobenzene fragment and phenanthro[9,10-d]imidazole group[23], transducing the reduction reaction to fluorescence signals (Scheme S1, Figure 1B). Zn-**MPB**, an M_3L_3 capsule, was synthesized by a combination of Zn^{2+} with the two-arm tridentate ligands which contained niacinamide skeletons for efficiently promoting electron transfer (Scheme S2 and Figure 1A). It comprised three alternating connected ligands and three Zn^{2+} ions that each coordinated to two tridentate chelators from two different ligands. The amide moieties of the ligands provide hydrogen bonding sites for stable binding of **L-NO$_2$** inside Zn-**MPB** and a hydrophilic environment in cell-targeted delivery[24]. The three NADH mimics in the ligand backbones of Zn-**MPB** acted as electron carriers with bioaffinity, providing adequate electrons and protons to reduce the nitro group[25] of **L-NO$_2$**, since reduction of one nitro group requires six-electrons from three NADH cofactors.

The electrospray ionization-mass spectrometry results for Zn-**MPB** in acetonitrile showed an intense peak at *m/z* = 942.54 (Figure 1A) assigned to $[H_2Zn_3(MPB)_3]^{2+}$ species, suggesting the high stability of capsule [26]. After adding an equimolar amount of **L-NO$_2$**, an $H_2Zn_3(MPB)_3(L\text{-}NO_2)]^{2+}$ species appeared at *m/z* = 1166.17, revealing the formation of a 1:1 stoichiometric host-guest species, Zn-**MPB⊃L-NO$_2$** (Figure 1C). Moreover, the formation of Zn-**MPB⊃L-NO$_2$** species was demonstrated by the significant H-H interactions between the H atom (N-H) of **L-NO$_2$** and other H atoms from Zn-**MPB** (Figure 1E, S24). Next, we conducted the microcalorimetry titration of Zn-**MPB** (0.1 mM) with **L-NO$_2$** (1 mM) in DMSO Tris-HCl solution (v/v, DMSO 90%) (Figure S26A). The titration results showed formation of the 1:1 inclusion complex Zn-**MPB⊃L-NO$_2$**[27], for which the free energy of binding between Zn-**MPB** and **L-NO$_2$** was calculated as -9.43 kcal/mol. The binding constant (K_a) was calculated as 8.33×10^6 M^{-1}, which indicated the preferred formation and stable existence of host-guest systems[28]. UV-vis titration experiment of Zn-**MPB** and **L-NO$_2$** was also conducted in the same DMSO Tris-HCl solution (Figure S25E), and the calculation result of K_a value was $1.70\text{x}10^6$ M^{-1}, which matched with the microcalorimetry titration result and indicated Zn-**MPB⊃L-NO$_2$** could exist stably in aqueous solution.

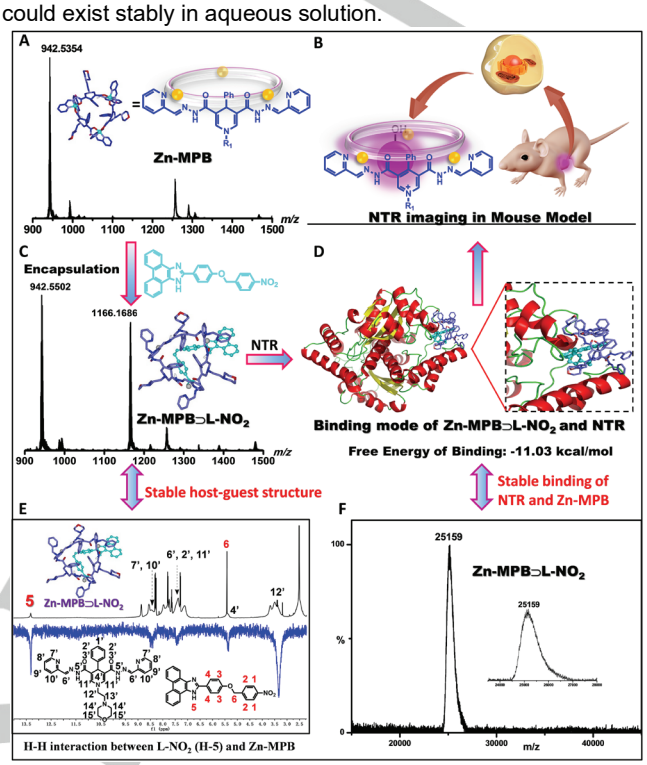

Figure 1. A) Self-assembly of ligands with Zn^{2+} to form Zn-**MPB**. B) Strategy for detection of NTR with a cofactor-substrate-based supramolecular luminescent probe. C) ESI mass spectrum of Zn-**MPB⊃L-NO$_2$**. D) Binding model of Zn-**MPB⊃L-NO$_2$** with NTR. E) H-H interaction between H-5 of L-**NO$_2$** and other H of Zn-**MPB** in deuterated DMSO-*d6*. F) The MALDI-TOF MS of Zn-**MPB**-NTR complex showed $[M+H^+]$ = 25159.

Docking calculations[20b] were carried out to obtain additional information regarding the intermolecular interaction between the host-guest platform and NTR. The substrate-based luminescent probe **L-NO$_2$** was bound in the pocket of NTR *via* hydrophobic and other intermolecular interactions. Hydrogen bonds formed between the O and N atoms of **L-NO$_2$** and amino acid residues generating intermediate state that exhibited free energy of binding about -8.78 kcal/mol between NTR and **L-NO$_2$**. Comparatively, Zn-**MPB⊃L-NO$_2$** was attached to the surface of **NTR** binding pocket, giving a free energy of binding of -11.03 kcal/mol (Figure 1D), which showed the formation of Zn-**MPB⊃L-NO$_2$**-NTR and a strong electron-donating system. Moreover, the MALDI-TOF MS of NTR showed a $[M+H^+]$ peak at 24715 (Figure S27). After binding with Zn-**MPB**, the MS dates showed a new peak 25159 (Figure 1F) that was attributed to the NTR species with the losing of an FMN ($C_{17}H_{20}N_4NaO_9P$, M = 478.3), an NADH ($C_{21}H_{27}N_7Na_2O_{14}P_2$, M = 709.4) and 14 H_2O, indicating the stable binding behaviour of Zn-**MPB** with NTR.

Besides, the UV-vis absorption titration (Figure S25A-S25C) and the microcalorimetry titration (Figure S26B) tests of NTR with Zn-MPB were conducted to verify the sable binding of NTR and Zn-**MPB**, of which the binding constants were calculated as $1.30\text{x}10^6$ M^{-1} or 1.92×10^6 M^{-1}, respectively. The result confirmed the stability of the Zn-**MPB** contained NTR, demonstrating the

possible application of the cofactor-substrate-based supramolecular luminescent probe *in vitro* and *in vivo*.

When excited at 468 nm in Tris-HCl buffer (10.0 mM, pH 7.4, 25℃), fluorescence spectra of Zn-**MPB⊃L-NO₂** or NTR exhibited no obvious emission from 490 to 670 nm. After adding NTR to Zn-**MPB⊃L-NO₂**, an emission peak rapidly appeared and increased at 530 nm with the increasing addition of NTR (Figure 2B). The biomimetic catalytic reaction quickly reached equilibrium within 5 s (Figure 2D, S29, S30B, S31A). The corresponding emission band was assigned to **L'-OH** according to the reported the reduction conversion of **L-NO₂** into **L'-OH** (Figure S33).[20a,29] Zn-**MPB⊃L-NO₂** showed good linear relationship with an approximately equal slope between enzyme content and fluorescence intensity independent of time changes (Figure 2F), ensuring quantitative analysis of NTR.

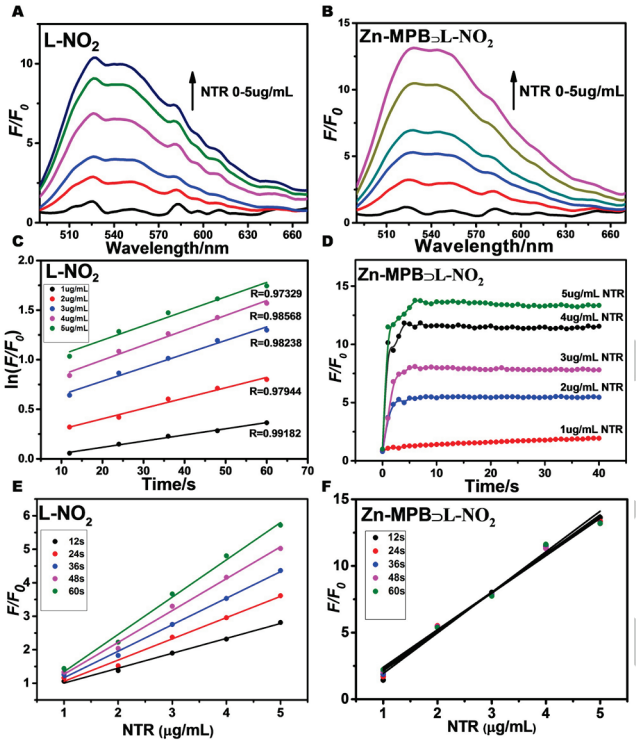

Figure 2. A, B) Fluorescence spectra showing reaction of NTR with **L-NO₂** (5 μM) and NADH (15 μM) or Zn-**MPB⊃L-NO₂** (5 μM). C, D) Time-dependent intensity variation of **L-NO₂** (5 μM) with NADH (15 μM) or Zn-**MPB⊃L-NO₂** (5 μM) in NTR. E, F) Intensity vs. NTR levels in 5 μM **L-NO₂** and 15 μM NADH or Zn-**MPB⊃L-NO₂** (5 μM) at different times.

In contrast, control experiments (Figure 2A, 2C, 2E) based on traditional probe **L-NO₂,** by adding different amounts of NTR to **L-NO₂** and NADH mixed solution, displayed similar emission peaks as the solution above. Nevertheless, **L-NO₂** reached equilibrium over 10 min (Figure S30A, S31B), which spent over 100-fold reaction time longer than that of Zn-**MPB⊃L-NO₂**. The slower reaction of **L-NO₂** with NTR made the plots and slopes of the intensity *vs.* NTR content keep altering over time (Figure 2E), which made it hard to work out the enzyme concentration. Zn-**MPB⊃L-NO₂** improved NTR detection with significantly shorter reaction time and higher sensitivity. Further tests found increase of NADH had significant influences on **L-NO₂** reduction by NTR (Figure S30A), expectedly showing increasing in initial rates and significant changes at equilibrium emission intensity, which means NTR detection is severely dependent on NADH supply. While, the reaction between Zn-**MPB⊃L-NO₂** and NTR hardly changed with/without addition of NADH before or after the reaction (Figure S29, S30B). Such an NADH independent behavior of Zn-**MPB⊃L-NO₂** system was postulated to be beneficial the quickly detecting and accuracy imaging NTR *in vivo*.

It is well-known that the reduction of nitro group by NADH and NTR is a typically double-substrate enzymatic reaction[13]. While, the new reporter, Zn-**MPB⊃L-NO₂**, responded to the NTR concentration rarely affected by the NADH supply, and signal communication occurred in a pseudo-intramolecular manner, simplifying the double-substrate mechanism[30] into a single-substrate[31] free collision mechanism. In the presence of various concentrations of **L-NO₂** or Zn-**MPB⊃L-NO₂** with a specific content of NTR (Figure S31, S32), the kinetic parameters calculated by the Michaelis–Menten equation[32] exhibited $V_{max}^{\text{Zn-MPB⊃L-NO2}}/V_{max}^{\text{L-NO2}}$ and $k_{cat}^{\text{Zn-MPB⊃L-NO2}}/k_{cat}^{\text{L-NO2}}$ values of about 100. Our new single-substrate free collision mechanism showed that the maximum reaction rate and TON of our Zn-**MPB⊃L-NO₂** were enhanced by *ca.* 100-fold. Compared to a natural catalytic system, Zn-**MPB⊃L-NO₂** improved catalytic efficiency by changing the catalytic kinetics.

Considering the complexity of the intracellular environment, **L-NO₂** and Zn-**MPB⊃L-NO₂** were treated with various potential interfering analytes in Tris-HCl buffer, such as glucose (50 mM), dithiothreitol (DTT 10 mM), amino acids (1 mM D-Glu, L-Tyr, L-Pro, L-Arg, L-Asp, and H-Cys-OH·HCl respectively) and bovine serum albumin (BSA 1 μg/mL) (Figure 3D). These interfering species induced no obvious fluorescence changes, showing a high selectivity and specificity of **L-NO₂** and Zn-**MPB⊃L-NO₂** for NTR over other intracellular species. Noted that the addition of NTR to the solution containing interfering analyte and Zn-**MPB⊃L-NO₂** immediately caused the similar fluorescent response to that of Zn-**MPB⊃L-NO₂** solution, indicating the good detection for NTR under complex conditions. Moreover, Zn-**MPB** and Zn-**MPB⊃L-NO₂** were tested in cell media and plasma, the dates showed that the fluorescence intensity (λ_{ex} = 375 nm) of Zn-**MPB** changed little over times (Figure S28). These results demonstrated that the cofactor-substrate-based supramolecular probe might be a promising tool to be applied for ultrafast detection of NTR in living organisms.

Further CCK-8 (Cell Counting Kit-8) assays[33] were carried out to evaluate biocompatibility. The cell viability of MCF-7, MDA-MB-231, and A549 cells was over 80% after pre-incubation with various concentrations of the substrate **L-NO₂** and Zn-**MPB** (1–20 μM) for 24 h, revealing the low cytotoxicity of **L-NO₂** and Zn-**MPB** in organisms (Figure S34). These results indicated the capabilities of **L-NO₂** and Zn-**MPB⊃L-NO₂** for NTR imaging and kinetic monitoring *in vivo*. To study intracellular fluorescence imaging of NTR, cells were incubated at 37℃ under normoxic (20% O_2) or hypoxic conditions (8% or 0.1%) [34,35] and imaged at various reaction times. As shown in Figure 3A, MCF-7 cells were incubated in different oxygen levels treatment for 6 h before the tests. Because **DMPDD**(dimethyl 1-(2-morpholinoethyl)-4-phenyl -1,4-dihydro-pyridine-3,5-dicarboxylate, named **compound 4** in Scheme S2) has the similar NADH mimics structure and didn't contain any coordinating groups, it could not formed capsule

structure and guaranteed as the reference compound in the bio-imaging experiments. After MCF-7 cells were incubated with Zn-**MPB⊃L-NO₂** or **L-NO₂** or **L-NO₂-DMPDD** (Figure 3) for 1 min, cells were subjected to confocal microscopy. The fluorescence intensity of cells increased with the degree of hypoxia. Additionally, intensity of cells incubated with Zn-**MPB⊃L-NO₂** was much stronger than that incubated with **L-NO₂** or **L-NO₂-DMPDD** at the same oxygen content, which could be identified by direct observation. We also did the cell control experiments with Co^{2+} treatment[36] which showed that the addition of Co^{2+} caused moderate hypoxia (approximately similar effects with that of 8% O_2 groups) as a result of the binding of Co^{2+} with hypoxia-inducible factor (HIF). These phenomena were also consistently observed in A549 and MDA-MB-231 cells (Figure S35, S36), showing the better intracellular NTR imaging capability of Zn-**MPB⊃L-NO₂** compared to the traditional probe platform **L-NO₂**.

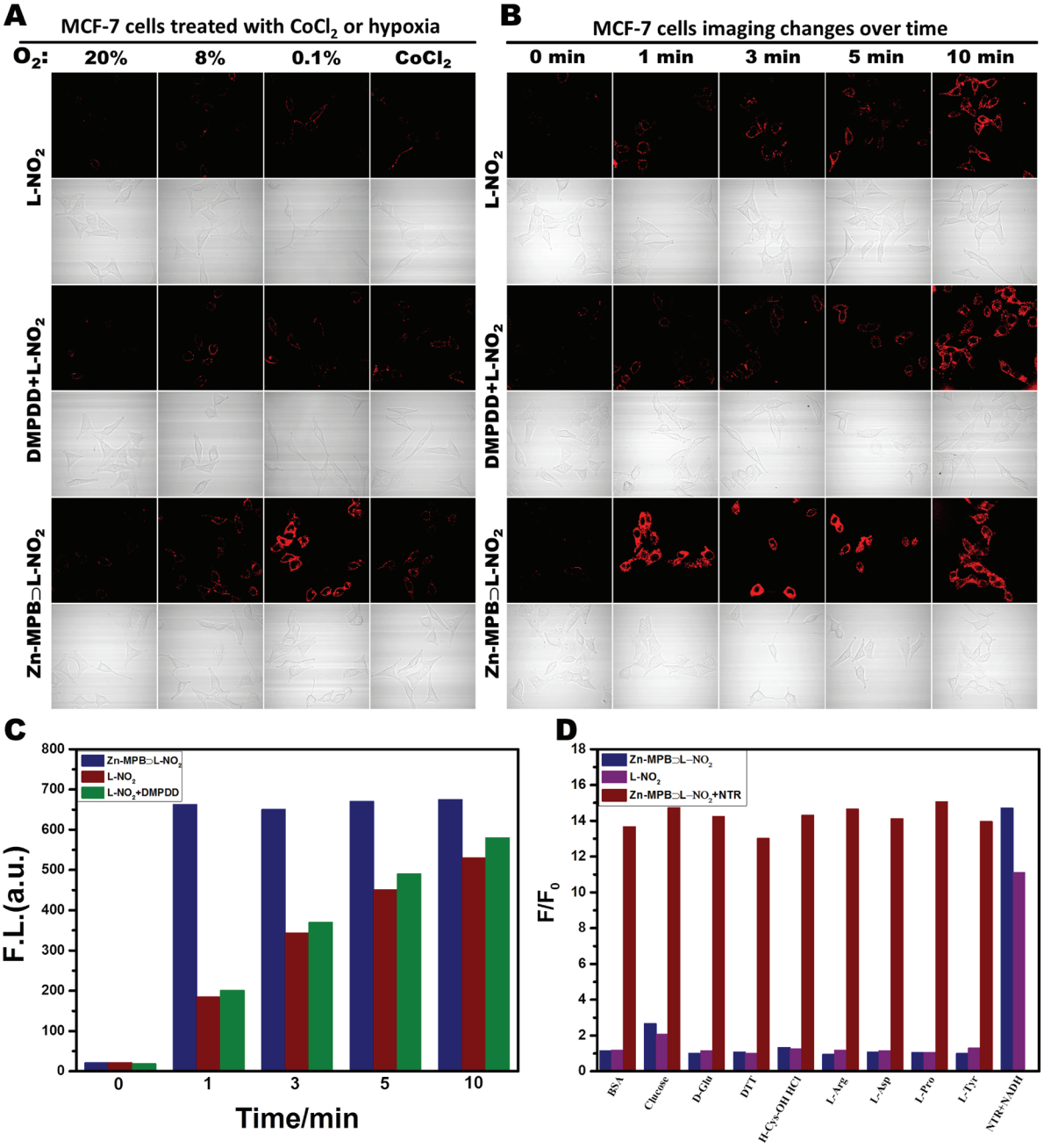

Figure 3. A) Imaging of MCF-7 cells treated with 1 μM **L-NO₂**, 1 μM **L-NO₂** with 3 μM **DMPDD** or 1 μM Zn-**MPB⊃L-NO₂** for 1 min after the 6 h incubation in different hypoxia or $CoCl_2$ conditions. B) Imaging of MCF-7 cells in 0.1% O_2 groups incubated with 1 μM **L-NO₂**, 1 μM **L-NO₂** with 3 μM **DMPDD** or 1 μM Zn-**MPB⊃L-NO₂** for different times (0, 1, 3, 5, 10 min). C) Cellular fluorescence intensity changes after treatment with 1 μM **L-NO₂** (wine columns), 1 μM **L-NO₂** with 3 μM **DMPDD** (green columns) or 1 μM Zn-**MPB⊃L-NO₂** (blue columns) for different times. D) Fluorescence intensity changes for 5 μM **L-NO₂** (with 15 μM NADH, purple columns) or Zn-**MPB⊃L-NO₂** (5 μM, blue columns) in Tris-HCl solution among the interfering analytes (date were recorded for 10 min, until **L-NO₂** groups reached equilibrium); And after adding NTR (5 μg/ml) to the Zn-**MPB⊃L-NO₂** (5 μM) in present of various interfering analyte mixture solutions, the fluorescence intensity reached equilibrium in seconds (wine columns).

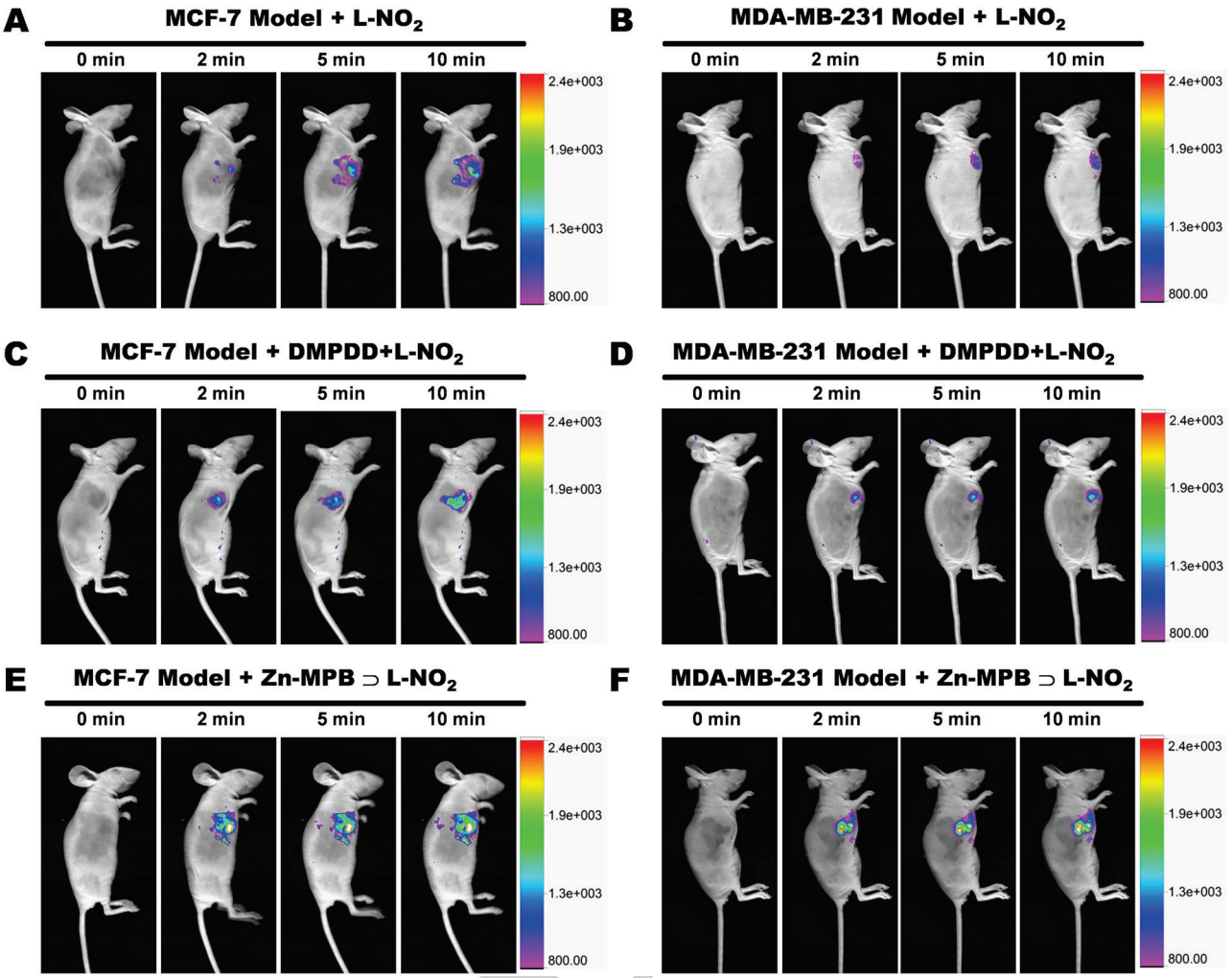

Figure 4. A, C, E) Bio-imaging of MCF-7 tumor-bearing mice at various times after injection with **L-NO$_2$**, **L-NO$_2$-DMPDD** or Zn-**MPB⊃L-NO$_2$**. B, D, F) Bio-imaging of MDA-MB-231 tumor-bearing mice at various times after injection with **L-NO$_2$**, **L-NO$_2$-DMPDD** or Zn-**MPB⊃L-NO$_2$**.

Further studies on intracellular catalytic kinetics[37,38] of NTR in MCF-7 cells with Zn-**MPB⊃L-NO$_2$** or **L-NO$_2$** or **L-NO$_2$-DMPDD** were conducted under hypoxic conditions (0.1% O_2) with different incubation times (Figure 3B, 3C). Fluorescence images of cells were obtained in the red channel at 508–608 nm and λ_{ex} = 488 nm. Surprisingly, the fluorescence in Zn-**MPB⊃L-NO$_2$** experimental groups rapidly reached equilibrium even with 1 min incubation time, and the fluorescence images of cells exhibited no apparent changes during longer incubation time (1–10 min) (Figure 3B and 3C). In contrast, the fluorescence of **L-NO$_2$** or **L-NO$_2$-DMPDD** control groups was only slightly enhanced with increasing cell incubation time, and even after 10 min of incubation, the fluorescence intensity of cells remained unequilibrium and was weaker than that of Zn-**MPB⊃L-NO$_2$**. A similar tendency was also exhibited by MDA-MB-231 and A549 cells (Figure S35, S36). These results demonstrated that Zn-**MPB⊃L-NO$_2$** was a rapid and efficient method for intracellular NTR imaging and verified that the cofactor-substrate-based supramolecular could help improve the double-substrate mechanism to a single-substrate one.

Additionally, mice were used to monitor and trace the NTR catalytic kinetics with Zn-**MPB⊃L-NO$_2$**. Mice fluorescent imaging[39,40] tests were excited at 470 nm and collected at 530 nm by Bruker In Vivo F Pro system. MCF-7 and MDA-MB-231 tumor-bearing mice were used to conduct the small animal fluorescence imaging experiments of Zn-**MPB⊃L-NO$_2$** *in vivo* and explore the fluorescence signal changes over time (Figure 4A-4F). While, **L-NO$_2$** or **L-NO$_2$-DMPDD** were used as control groups for the investigation of imaging capability of our cofactor-substrate-based supramolecular probe. Rapid fluorescence enhancement of Zn-**MPB⊃L-NO$_2$** groups was shown in the tumor region of tumor-bearing mice, which reached equilibrium within 10 min, and exhibited considerable increase in intensity compared with L-**NO$_2$** groups or **L-NO$_2$-DMPDD** groups. Alternatively, the latter two control groups showed much weaker fluorescence imaging in the tumor region and the intensity reached equilibrium for over 10 min, showing a longer time than that of Zn-**MPB⊃L-NO$_2$**. These results demonstrated that Zn-**MPB⊃L-NO$_2$** exhibited excellent performance for rapid NTR imaging and enzymatic kinetics monitoring *in vivo*.

Conclusion

In summary, a cofactor-substrate-based supramolecular luminescent probe, Zn-**MPB**⊃L-**NO₂**, for the ultrafast quantitative detection and bio-tracking of hypoxic NTR was constructed by encapsulating a substrate-based fluorescent probe **L-NO₂** within the NADH mimic-containing metal-organic capsule Zn-**MPB**. Zn-**MPB**⊃L-**NO₂** forced the NADH mimic capsule into proximity with **L-NO₂**, facilitated a unique NADH-independent NTR's detection, enabling the enzyme catalysis to switch from the original complex double-substrate process to a single-substrate one. The new signalling communication method ensures a linear relationship between NTR content and fluorescence intensity with an ultrafast equilibrium of seconds in solution detection, It guarantees the biotracing of NTR in cells and mice more quickly than the traditional probes, demonstrating the superiority of this approach over traditional methods in NTR imaging and early tumor diagnosis. The advantage of the cofactor-substrate-based supramolecular luminescent probe for fusion of cofactor and luminescent substrate endows a new and promising method in bioimaging and biomimetic catalysis.

Acknowledgements

This research was financially supported by the NSFC (No 21820102001 and 21977015). We acknowledge Associate Professor Jiqiu Yin (from Dalian Medical University) for the aid of small animal experiments.

Keywords: Metal-organic capsule • Supramolecular probe • Cofactor mimic • Hypoxia enzyme • Ultrafast detection

[1] D. M. Gilkes, G. L. Semenza, D. Wirtz, *Nat. Rev. Cancer* **2014**, *14*, 430-439.

[2] a) A. T. Henze, M. Mazzone, *J. Clin. Invest.* **2016**, *126*, 3672-3679; b) L. Y. Ye, W. Chen, X. L. Bai, X. Y. Xu, Q. Zhang, X. F. Xia, X. Sun, G. G. Li, Q. D. Hu, Q. H. Fu, T. B. Liang, *Cancer Res.* **2016**, 76, 818-830.

[3] a) H. Choudhry, A. L. Harris, *Cell Metab.* **2018**, 27, 281-298; b) G. Z. Qiu, M. Z. Jin, J. X. Dai, W. Sun, J. H. Feng, W. L. Jin, *Trends Pharmacol. Sci.* **2017**, 38, 669-686.

[4] a) S. C. Yang, Z. H. Tang, C. Y. Hu, D. W. Zhang, N. Shen, H. Y. Yu, X. S. Chen, *Adv. Mater.* **2019**, *31*, 1805955; b) L. J. O'Connor, C. Cazares-Körner, J. Saha, C. N. G. Evans, M. R. L. Stratford, E. M. Hammond, S. J. Conway, *Nat. Protoc.* **2016**, 11, 781-794.

[5] a) J. N. Liu, W. B. Bu, J. L. Shi, *Chem. Rev.* **2017**, *117*, 6160-6224; b) H. W. Liu, L. L. Chen, C. Y. Xu, Z. Li, H. Y.Zhang, X. B. Zhang, W. H. Tan, *Chem. Soc. Rev.* **2018**, 47, 7140-7180.

[6] a) H. J. Knox, J. Hedhli, T. W. Kim, K. Khalili, L. W. Dobrucki, J. Chan, *Nat. Commun.* **2017**, *8*, 1794; b) W. Piao, K. Hanaoka, T. Fujisawa, S. Takeuchi, T. Komatsu, T. Ueno, T. Terai, T. Tahara, T. Nagano, Y. Urano, *J. Am. Chem. Soc.* **2017**, 139, 13713-13719.

[7] X. H. Zhu, M. Lu, B. Y. Lee, K. Ugurbil, W. Chen, *P.N.A.S.* **2015**, *112*, 2876–2881.

[8] a) Y. P. Wang, K. Y. San, G. N. Bennett, *Curr. Opin. Biotech.* **2013**, 24, 994-999; b) C. K. Prier, F. H. Arnold, *J. Am. Chem. Soc.* **2015**, 137, 13992−14006.

[9] M. Richter, *Nat. Prod. Rep.* **2013**, 30, 1324-1345.

[10] M. H. Lee, A. Sharma, M. J. Chang, J. Lee, S. Son, J. L. Sessler, C. Kang, J. S. Kim, *Chem. Soc. Rev.* **2018**, 47, 28-52.

[11] A. Kaur, E. J. New, *Acc.Chem.Res.* **2019**, 52, 623−632.

[12] W. W. Chen, E. Freinkman, T. Wang, K. Birsoy, D. M. Sabatini, *Cell* **2016**, 166, 1324–1337.

[13] P. R. Race, A. L. Lovering, R. M. Green, A. Ossor, S. A. White, P. F. Searle, C. J. Wrighton, E. I. Hyde, *J. Biol. Chem.* **2005**, 280, 13256-13264.

[14] a) T. R. Cook, P. J. Stang, *Chem. Rev.* **2015**, 115, 7001-7045; b) C. J. Brown, F. D. Toste, R. G. Bergman, K. N. Raymond, *Chem. Rev.* **2015**, 115, 3012−3035.

[15] L. J. Jongkind, X. Caumes, A. P. T. Hartendorp, J. N. H. Reek, *Acc. Chem. Res.* **2018**, 51, 2115−2128.

[16] a) K. K. Yan, M. Fujita, *Science* **2015**, 350, 1165-1166; b) S. T. Bai, C. B. Bheeter, J. N. H. Reek, *Angew. Chem. Int. Ed.* **2019**, 58, 2696-2699.

[17] W. C. Geng, S. Y. Jia, Z. Zheng, Z. H. Li, D. Ding, D. S. Guo, *Angew. Chem. Int. Ed.* **2019**, 58, 2377-2381.

[18] W. Cullen, M. C. Misuraca, C. A. Hunter, N. H. Williams, M. D. Ward, *Nat. Chem.* **2016**, 8, 231–236.

[19] a) X. D. Wang, H. H. P. Yiu, *ACS Catal.* **2016**, 6, 1880−1886; b) D. V. Titov, V. Cracan, R. P. Goodman, J. Peng, Z. Grabarek, V. K. Mootha, *Science* **2016**, 352, 231-235.

[20] a) A, Chevalier, Y, M. Zhang, O, M. Khdour, J. B. Kaye, S. M. Hecht, *J. Am. Chem. Soc.* **2016**, 138, 12009-12012; b) Y. H. Li, Y. Sun, J. C. Li, Q. Q. Su, W. Yuan, Y. Dai, C. M. Han, Q. H. Wang, W. Feng, F. Y. Li, *J. Am. Chem. Soc.* **2015**, 137, 6407−6416.

[21] Z. Thiel, P. Rivera-Fuentes, *Angew. Chem. Int. Ed.* **2019**, 58, 11474-11478.

[22] Z. J. Wang, K. N. Clary, R. G. Bergman, K. N. Raymond, F. D. Toste, *Nat. Chem.* **2013**, 5, 100-103.

[23] J. M. Han, M. Xu, B. Wang, N. Wu, X. M. Yang, H. R. Yang, B. J. Salter, L. Zang, *J. Am. Chem. Soc.* **2014**, 136, 5090-5096.

[24] J. Rodríguez, J. Mosquera, J. R. Couceiro, J. R. Nitschke, M. E. Vázquez, J. L. Mascareñas, *J. Am. Chem. Soc.* **2017**, 139, 55−58.

[25] N. Hannink, S. J. Rosser, C. E. French, A. Basran, J. A. H. Murray, S. Nicklin, N. C. Bruce, *Nat. Biotechnol.* **2001**, 19, 1168-1172.

[26] M. M. Zhang, M. L. Saha, M. Wang, Z. X. Zhou, B. Song, C. J. Lu, X. Z. Yan, X. P. Li, F. H. Huang, S. C. Yin, P. J. Stang, *J. Am. Chem. Soc.* **2017**, 139, 5067-5074.

[27] P. J. Altmann, A. Pöthig, *J. Am. Chem. Soc.* **2016**, 138, 13171−13174.

[28] R. N. Dsouza, U. Pischel, W. M. Nau, *Chem. Rev.* **2011**, 111, 7941-7980.

[29] Y. C. Liu, L. L. Teng, L. L. Chen, H. C. Ma, H. W. Liu, X. B. Zhang, *Chem. Sci.* **2018**, 9, 5347-5353.

[30] T. L. Grove, J. S. Benner, M. I. Radle, J. H. Ahlum, B. J. Landgraf, C. Krebs, S. J. Booker, *Science* **2011**, 332, 604-607.

[31] F. Wong, A. Dutta, D. Chowdhury, J. Gunawardena, *P.N.A.S.* **2018**, 115, 9738–9743.

[32] a) M. Rabe, S. R. Tabaei, H. Zetterberg, V. P. Zhdanov, F. Hook, *Angew. Chem. Int. Ed.* **2015**, 54, 1022-1026; b) S. Bhakta, A. Nayek, B. Roy, A. Dey, *Inorg. Chem.* **2019**, 58, 2954-2964.

[33] X. J. Liu, Q. L. Feng, A. Bachhuka, K. Vasilev, *ACS Appl. Mater. Interfaces* **2014**, 6, 9733−9741.

[34] a) W. Piao, S. Tsuda, Y. Tanaka, S. Maeda, F. Y. Liu, S. Takahashi, Y. Kushida, T. Komatsu, T. Ueno, T. Terai, T. Nakazawa, M. Uchiyama, K. Morokuma, T. Nagano, K. Hanaoka, *Angew. Chem. Int. Ed.* **2013**, 52, 13028-13032; b) M. Batie, J. Frost, M. Frost, J. W. Wilson, P. Schofield, S. Rocha, *Science* **2019**, 363, 1222-1226.

[35] X. C. Zheng, H. Mao, D. Huo, W. Wu, B. R. Liu, X. Q. Jiang, *Nat. Biomed. Eng.* **2017**, 1, 0057.

[36] a) Y. Yuan, G. Hilliard, T. Ferguson, D. E. Millhorn, *J. Biol. Chem.* **2003**, 278, 15911-15916; b) Y. Yuan, D. Beitner-Johnson, D. E.Millhorn, *Biochem. Bioph. Res. Co.* **2001**, 288, 849–854.

[37] a) Z. Q. Xu, X. T. Huang, X. Han, D. Wu, B. B. Zhang, Y. Tan, M. J. Cao, S. H. Liu, J. Yin, J. Yoon, *Chem* **2018**, 4, 1609-1628; b) V. E. Zwicker, B. L. Oliveira, J. H. Yeo, S. T. Fraser, G. J. L. Bernardes, E. J. New, K. A. Jolliffe, *Angew. Chem. Int. Ed.* **2019**, 58, 3087-3091.

[38] J. B. Grimm, A. K. Muthusamy, Y. J. Liang, T. A. Brown, W. C. Lemon, R. Patel, R. W. Lu, J. J. Macklin, P. J. Keller, N. Ji, L. D. Lavis, *Nat. Methods* **2017**, 14, 987-994.

[39] a) W. W. An, L. S. Ryan, A. G. Reeves, K. J. Bruemmer, L. Mouhaffel, J. L. Gerberich, A. Winters, R. P. Mason, A. R. Lippert, *Angew. Chem. Int. Ed.* **2019**, 58, 1361-1365; b) S. Son, M. Won, O. Green, N. Hananya, A. Sharma, Y. Jeon, J. H. Kwak, J. L. Sessler, D. Shabat, J. S. Kim, *Angew. Chem. Int. Ed.* **2019**, 58, 1739-1743.

[40] a) K. J. Bruemmer, O. Green, T. A. Su, D. Shabat, C. J. Chang, *Angew. Chem. Int. Ed.* **2018**, 57, 7508-7512; b) A. D. Shao, Y. S. Xie, S. J. Zhu, Z. Q. Guo, S. Q. Zhu, J. Guo, P. Shi, T. D. James, H. Tian, W. H. Zhu, *Angew. Chem. Int. Ed.* **2015**, 54, 7275-7280.

10.1002/anie.201915040

WILEY-VCH

Entry for the Table of Contents (Please choose one layout)

RESEARCH ARTICLE

We propose a cofactor-substrate-based supramolecular probe strategy for ultrafast (within seconds) and quantitative hypoxia detection of NTR

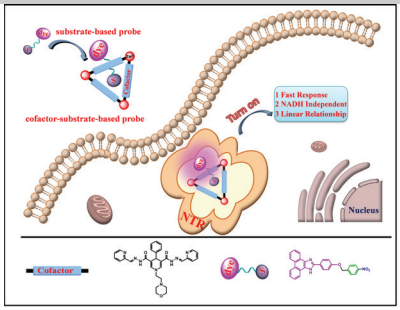

*Yang Jiao, Lei Zhang, Xu Gao, Wen Si and Chunying Duan**

Page No. – Page No.

Cofactor-substrate-based Reporter for Enhancing Signalling Communications towards Hypoxia Enzyme Expression